Desalination and Water Treatment
www.deswater.com
41 (2012) 122–130
March
1944-3994/1944-3986 © 2012 Desalination Publications. All rights reserved
doi: 10.1080/19443994.2012.664697
Taylor & Francis
Taylor & Francis Group

Adsorption of Cd(II) on lotus stalks-derived activated carbon: batch and column studies

LiHui Huang[a,c,*], YuanYuan Sun[a], QianKun Yue[b], Qinyan Yue[a], Li Li[a], Baoyu Gao[a]

[a]*Shandong Key Laboratory of Water Pollution Control and Resource Reuse, School of Environmental Science and Engineering, Shandong University, 27th South Shanda Roud, Jinan, Shangdong 250100, China*
Tel. +86 531 88366873; Fax: +86 531 88364513; email: huanglihui9986@126.com
[b]*College of Environmental and Natural Resource Sciences, Zhejiang University, Hangzhou 310029, China*
[c]*Shandong Dalong Industrial Limited Liability Company, Jinan 250100, China*

Received 1 July 2011; Accepted 30 January 2012

ABSTRACT

This paper reports a study of adsorption of Cd(II) from aqueous solutions using activated carbon made from lotus stalks (LSAC). The properties of LSAC were characterized by scanning electron microscopy and BET surface area. Zeta potential was also determined. The batch Cd(II) adsorption on LSAC was performed to study the different sorption parameters (time, pH, temperature and ionic strength) that influence the adsorption of Cd(II) onto LSAC and to explore the adsorption mechanisms. Bench-scale column tests were also carried out to determine breakthrough curves with varying flow rates and fixed-bed heights. In general, the theoretical q_e calculated using the pseudo-second-order kinetic model agreed better with the experimental data than the first-order one. Among the three widely-used isotherms (Langmuir, Freundlich, and Temkin models), the Langmuir model appeared to describe the experimental results best. The Adam–Bohart equation was appropriate for relative concentration ranging from 0.01 up to 0.5 in this study. The pH of the initial solution affected the sorption of Cd(II) on LSAC to the greatest extent, and presence of Mg^{2+} resulted in a larger competition to the active sites than Na^+, implying ion exchange and electrostatic attraction adsorption mechanisms.

Keywords: Activated carbon; Lotus stalks; Cd(II) adsorption; Breakthrough curve

1. Introduction

The serious incident of itai-itai disease was caused by cadmium poisoning in Japan. The harmful effects of Cd(II) ions include renal damage, hypertension, proteinuria, kidney stone formation, and testicular atrophy [1]. The conventional means for treating wastewaters containing cadmium are alkaline precipitation [2], ion exchange [3], membrane separation [4], electrodialysis [5], and adsorption [6,7]. Alkaline precipitation is effective only if the concentration of cadmium is high, but it creates secondary problems with metal-bearing sludge. The extensive utilization of ion exchange, membrane separation, and electrodialysis is restricted due to high maintenance costs. Attempts have been made to develop an inexpensive method which is simple, easy to operate and maintain [8]. Out of all the methods, the adsorption approach is optimum because of its sludge-free clean operation and effective for low-concentration contaminants [9]. Overall, activated carbons, which possess extensive surface area, high degree of surface reactivity, and favorable pore size distribution, are still commonly applied in environmental decontamination [10]. To overcome the

*Corresponding author.

disadvantage of high costs, numerous alternative precursors, such as discarded waste tyres [11], agricultural by-products [12,13], and hydrophytes [14], have been used for carbon production.

Hydrophytes are widely available and abundant natural materials because huge amounts of biomass are harvested periodically to keep the wetland ecosystem in good condition. Additionally, they have a porous system, which provides a good precondition for activated carbon. These properties may result in a good porous structure. Lotus, one kind of hydrophytes, is widely grown in Asia. Every year, lots of lotus stalks are disposed as solid waste, causing environmental problems.

In our previous study, we have applied lotus stalk-based activated carbon for Ni(II) adsorption [15]. To explore the selectivity of the adsorbate for particular cations and the feasibility for dynamic adsorption properties, we chose Cd(II) as another adsorbate. The objectives of the present study were: (1) to gain an understanding of the adsorption process kinetics and to evaluate the impacts of temperature, pH and ionic strength on Cd(II) removal, and (2) to determine the influence of flow rate and bed depth on Cd(II) removal in a column study.

2. Materials and methods

2.1. Preparation of the adsorbent

Lotus stalks activated carbon (LSAC) samples were obtained according to the method described elsewhere [14]. Lotus stalks, collected from Jinan (China), were washed with water to remove dust and dried at 80°C. Then, the materials were crushed to the desired size (2–3 mm) using a grinder. After impregnating with phosphoric acid (40 wt.%) in a ratio of 2:1(g H_3PO_4/g LS) for 12 h, the sample was transferred to a muffle furnace and kept at 450°C for 1 h. Afterwards, the mass was cooled to ambient temperature and washed with distilled water until the pH of the supernatant became steady (pH = 6.5), then crushed and sieved to 100–140 mesh by standard sieves. The adsorbent obtained was kept in desiccators for subsequent study.

2.2. Adsorbent characterization and analytical method

Samples of LSAC were scanned with a HITACHI S-520 (Japan) scanning electron microscope. Zeta potential of LSAC was determined by an electrokinetic analyzer (JS94H, Zhongchen Digital Technical Apparatus Co., Ltd., Shanghai, China). The specific surface area and pore size distributions of LSAC were measured by the nitrogen adsorption–desorption isotherm method using a surface area analyzer (Quantachrome Corporation, USA). The porous structure parameters were determined using the same methods described in literature [16]. Moreover, an atomic absorption spectrophotometer (AAS; 180-80, Polarized Zeeman, HITACHI) was used for Cd(II) concentrations. The pH of the solution was adjusted with concentrated HCl or NaOH solution (0.001–1 M), and measured with a pH meter (Model pHS-3C, Shanghai, China). Duplicate samples were carried out and the precision of the parallel measurements was ±5% relative standard deviation.

2.3. Batch studies

A standard stock solution of 1,000 mg/L was prepared by dissolving an appropriate amount of Cd $(NO_3)_2{\cdot}4H_2O$ (analytical grade) in distilled water. Working solutions of Cd(II) ions were prepared by diluting the stock solution. In batch studies, cadmium adsorption was measured as a function of pH, ionic strength and temperature. The ionic strength was separately adjusted to 0.05, 0.1, 0.2, 0.4 and 0.8 M using concentrated $NaNO_3$ and $Mg(NO_3)_2$ solution. LSAC (0.1 g) mixed with 100 mL Cd(II) solutions was shaken at 125 rpm under room temperature. After vibrating for suitable time in the oscillator, the samples were filtered through a membrane with a pore diameter of 0.45 μm and then the residual Cd(II) concentrations in supernatants were analyzed.

Adsorption kinetics experiments were conducted in a 1,000 mL beaker by dispersing LSAC (0.5 g/L, 1 g/L, 1.5 g/L) into 1,000 ml of working Cd(II) solutions (50 mg/L) with a background electrolyte (0.01 M NaCl). The pH of the solution was 5.4. Then, the beaker was placed on a magnetic stirrer (HJ-3, Jintan medical instrument corporation, China) at a speed of 125 rpm at a temperature of 25 ± 1°C. The samples were collected at pre-specified times to determine the residual concentrations.

2.4. Column studies

Fixed-bed column experiments were conducted to investigate the removal efficiency of Cd(II) by LSAC at room temperature (25 ± 1°C). Glass columns with an inner diameter of 0.8 cm were loaded with 0.6, 1.0 and 1.5 g of LASC. The LSAC was outgassed by impregnating it in deionized water overnight. The working solution containing 50 mg/L of Cd(II) was passed through the column in an up-flow direction at various flow rates (5, 10, 15 mL/min) using a peristal-

tic pump. The solution flowing through the column was collected at pre-specified time intervals and the samples were analyzed.

3. Results and discussion

3.1. Properties of LSAC

Fig. 1 shows the scanning electron microscope (SEM) photo of LSAC. Different from activated carbon derived from other materials, the typical feather of LSAC shows an accordant tubular structure. This configuration may favor the diffusion of Cd(II) into LSAC. The zeta potential of LASC was −35.1 mV, illustrating the existence of functional groups with negative charge on LSAC. This can help Cd(II) adsorption onto LSAC by electrostatic adherence. Characterization of LSAC is significant to the understanding of the textual characteristics that may affect the removal of metal ions. Fig. 2 shows the pore size distributions of LSAC, and the inset is the nitrogen adsorption and desorption isotherms at 77 K. The properties of activated carbon determined in this study are summarized in Table 1. According to the International Union of Pure and Applied Chemistry (IUPAC) classification adsorption isotherms, the nitrogen adsorption desorption isotherms of LSAC showed a mixture of types I and IV, suggesting that both micropores (type I) and mesopores (type IV) were well developed. The BET surface area of LSAC based on the isotherms was 1220 m^2/g which was relatively high for activated carbon. Visibly, LSAC exhibited a broad multimodal distribution with the highest peak at 1.41 nm, centered at the mic-mesopores region.

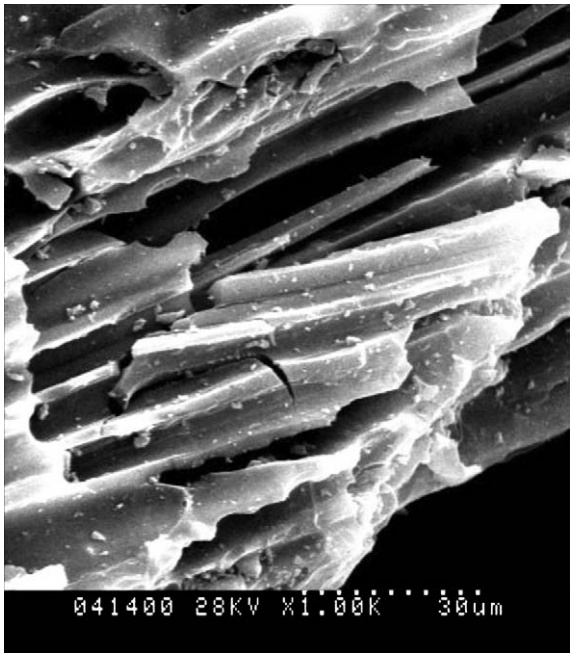

Fig. 1. SEM photo of LSAC (1,000×).

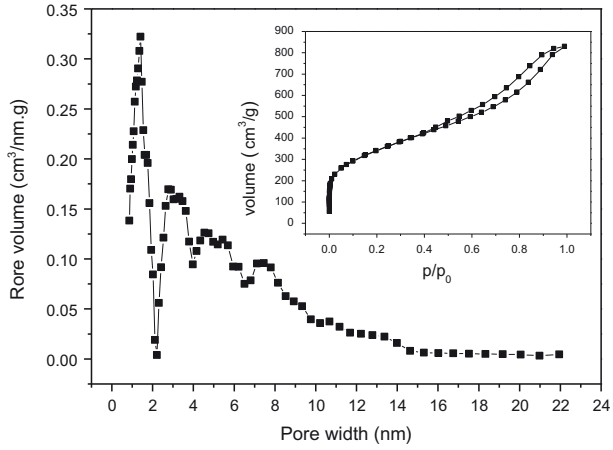

Fig. 2. Pore-size distribution of LSAC. The inset is the nitrogen adsorption–desorption isotherm plots of LSAC at 77 K [14].

3.2. Effect of the pH of the initial solution

Previous studies have shown that pH is one of the most significant parameters influencing heavy metal adsorption [17]. Adsorption of Cd(II) onto LSAC as a function of pH is shown in Fig. 3. It should be noted that the adsorption of Cd(II) by LSAC was highly pH dependent, and the removal capacity increased sharply from 8.875 to 32.38 mg/g with the increase of pH from 1.78 to 6.85. This phenomenon demonstrated that the adsorption mechanism of Cd(II) involved ion exchange [18]. Moreover, at the lower pH, the functional groups responsible for binding ions on the carbon surface were in the protonated form and higher electrostatic repulsion would lead to lower adsorption capacity. At a high pH, the competition of H^+ with the Cd^{2+} for the adsorption active sites on the LSAC was less; hence, adsorption of Cd(II) enhanced with increasing pH. Mohan and Singh [19] and Blázquez et al. [20] have reported similar results. In addition, the pH of the solution decreased during the adsorption progress, which was consistent with the ion-exchange mechanism discussed below. The H^+ bound to acidic functional groups can exchange with Cd^{2+}, resulting in an increase in the H^+ concentration.

3.3. Effect of ionic strength

Fig. 4 shows the effect of ionic strength on Cd(II) adsorption onto LSAC. As can be seen, the negative

Table 1
Porous structure parameters of LSAC [14]

S_{BET} (m^2/g)	S_{mic} (m^2/g)	(%)	S_{ext} (m^2/g)	(%)	V_{tot} (cm^3/g)	V_{mic} (cm^3/g)	(%)	V_{ext} (cm^3/g)	(%)	D_w nm
1220	502.71	41.2	717.29	58.8	1.191	0.2858	24	0.9052	76	1.41

S_{BET}: BET surface area, S_{mic}: micropore surface area, S_{ext}: external surface area, V_{tot}: total pore volume, V_{mic}: micropore volume, V_{ext}: external volume, D_w: pore width (Mode).

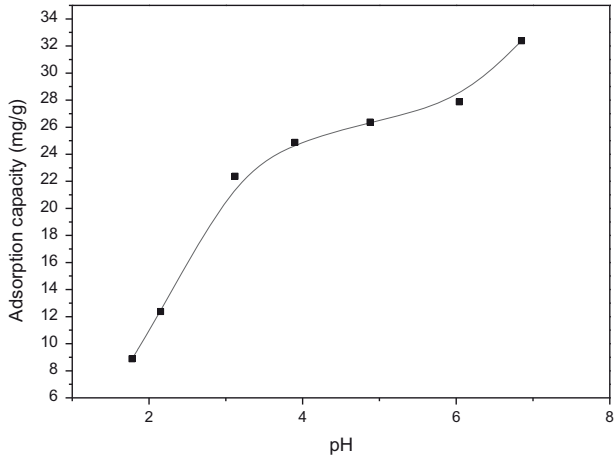

Fig. 3. Effect of the pH of the initial solution for the adsorption of Cd(II) onto LSAC ($C_0 = 50.0$ mg/L; pH = 5.4; $T = 25 \pm 1$°C; dosage 1.0 g/L; $t = 2$ h).

effect of $Mg(NO_3)_2$ on Cd(II) adsorption was much more obvious than that caused by $NaNO_3$ solution. The adsorption capacity reduced from the original 36.11 to 31.72 mg/L with increasing $NaNO_3$ concentration from 0 to 0.8 M. While, the adsorption capacity of Cd(II) decreased from 36.11 to 12.745 mg/g when $Mg(NO_3)_2$ increased from 0.0 to 0.8 M. Cd(II) removal was dependent on the concentration of ionic strength, indicating that Cd(II) removal was mainly by electrostatic interactions between the adsorbate and the adsorbent [21]. Thus, $Mg(NO_3)_2$ (divalent electrolyte) which has higher electric charge can cause a greater impact on Cd(II) adsorption.

3.4. Adsorption kinetics

The kinetics of Cd(II) adsorption onto LSAC at different dosages is shown in Fig. 5. The Cd(II) adsorption on LSAC was a rapid process and 30 min was sufficient to achieve equilibrium. With the driving force becoming weaker and active sites diminishing, the adsorption speed of Cd(II) on LSAC became slower and gradually approached an equilibrium position. It also can be seen from Fig. 5 that the dosage of LSAC has an important impact on Cd(II) adsorption. The Cd(II) removal efficiency increased while adsorption capacity decreased with an increasing dosage. This could be attributed to a smaller amount of LSAC dosage causing more competition for the active sites.

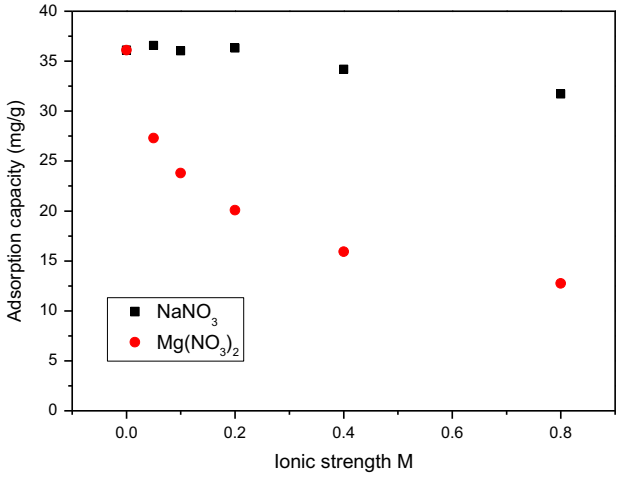

Fig. 4. Effect of ionic strength on Cd(II) removal by LSAC ($C_0 = 50.0$ mg/L; pH = 5.4; $T = 25 \pm 1$°C; dosage 1.0 g/L; $t = 2$ h).

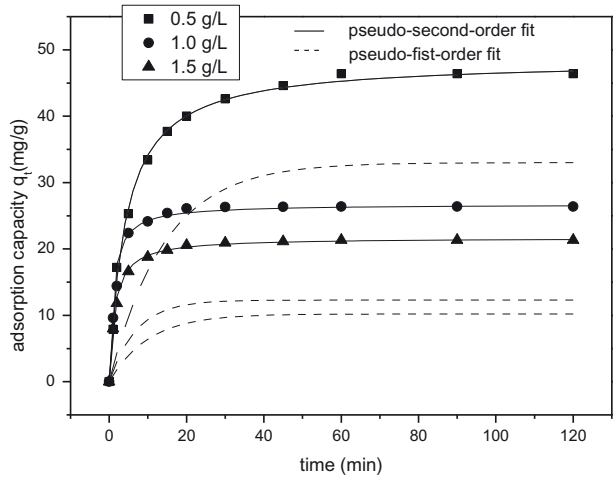

Fig. 5. Adsorption kinetics for Cd(II) removal using LSAC at different dosages and comparison of different kinetic models ($C_0 = 50$ mg/L; dosage = 0.5, 1.0, 1.5 g/L; initial pH = 5.4; temperature = 25 ± 1°C).

The validity of two models, pseudo-first and second-order kinetic model, was checked by studying the kinetics under different dosages. The pseudo-first-order equation can be represented as [22]:

$$\ln(q_e - q_t) = \ln q_e - k_1 t \quad (1)$$

where q_e and q_t (both in mg/g) are the amounts of Cd(II) adsorbed per unit mass of activated carbon at equilibrium and time t, respectively; k_1 is the pseudo-first-order adsorption rate constant (mg/g min). The values of k_1 and q_e were calculated from the plots of $\log(q_e - q_t)$ vs. t.

The pseudo-second-order equation can be expressed as follows [23,24]:

$$\frac{t}{q_t} = \frac{1}{k_2 q_e^2} + \frac{1}{q_e} t \quad (2)$$

where k_2 (g/mg min^{-1}) is the adsorption rate constant, k_2 and q_e (mg/g) values can be obtained from the intercept and slope of the plots of t/q_t vs. t.

Table 2 shows the kinetic data obtained from the pseudo-first and second-order kinetic models for the sorption of Cd(II) on LSAC. According to the correlation coefficient (R^2) values listed in the Table 2, the pseudo-second-order kinetics equation fit the test data better than the pseudo-first-order kinetics equation. The calculated q_e value was also in good agreement with the experimental results for the second-order kinetic model, suggesting that chemisorption was the dominant adsorption mechanism. These results were consistent with the observations of the effect of pH and ionic strength. The predicted adsorption amounts per unit mass were 48.426, 26.724, and 21.673 mg/g by the pseudo-second-order kinetics for solutions with LSAC dosages of 0.5, 1, and 2 g/L, respectively.

3.5. Adsorption isotherms

The isotherms for adsorption of the Cd(II) at pH 5.4 are presented in Fig. 6 for three different temperatures. The isotherms plots were concave to the concentration axis, suggesting that the increase in the uptake of Cd(II) became slower with an increase in concentration. The uptake of Cd(II) increased with temperature, thereby indicating that the process was endothermic. Adsorption isotherms are commonly used to represent equilibrium relationships between an adsorbent and an adsorbate. Three adsorption isotherm equations were applied in the present study namely, Langmuir, Freundlich, and Tempkin isotherms. The applicability of the isotherm models to the adsorption data were confirmed by comparing the value of the correlation coefficients.

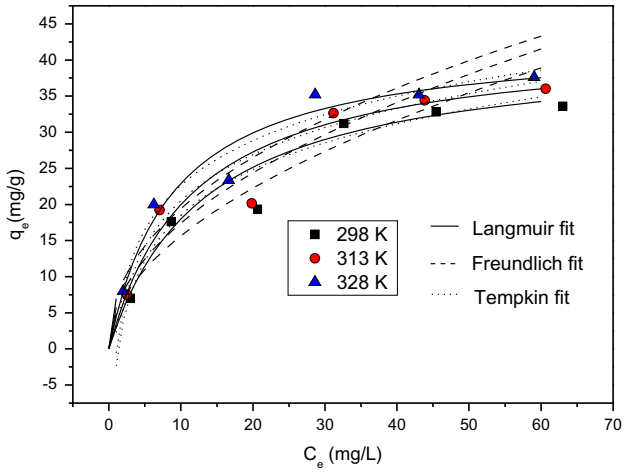

Fig. 6. Adsorption isotherms for Cd(II) removal using LSAC at different temperatures and comparison of different thermodynamic models ($C_0 = 50$ mg/L; LSAC dosage = 0.5, 1.0, 1.5 g/L; initial pH = 5.4; $T = 25 \pm 1$°C).

The Langmuir [25] theory assumes monolayer adsorption, with no lateral interaction and steric hindrance between the adsorbed molecules. The equation is given as follows:

$$\frac{C_e}{q_e} = \frac{1}{Q_0 K_l} + \frac{1}{Q_0} C_e \quad (3)$$

where C_e (mg/L) and q_e (mg/g) are the concentration of adsorbate and the amount of adsorbate adsorbed under equilibrium, respectively; K_l (L/mg) is the Langmuir adsorption constant and Q_0 (mg/g) is the maximum adsorption amount. Q_0 and K_l are deter-

Table 2
Estimated kinetic model parameters for Cd(II) adsorption

Dosage g/L	Experimental q_e,(mg/g)	Pseudo-first-order equation			Pseudo-second-order equation		
		$q_{e,cal}$ (mg/g)	k_1 (mg/g min)	R^2	$q_{e,cal}$ (mg/g)	k_2 (g/mg min)	R^2
0.5	46.4	33.00	0.0707	0.947	48.426	0.00493	0.998
1.0	26.4	12.29	0.1430	0.504	26.723	0.03664	0.999
2.0	21.35	10.20	0.0988	0.629	21.673	0.03321	0.999

mined from the slope and intercept of the plot of C_e/q_e vs. C_e.

Freundlich isotherm [26] assumes that multilayer adsorption has occurred, with non-uniform distribution of adsorption heat and affinities over the heterogeneous surface of the adsorbent. The Freundlich isotherm can be expressed as:

$$\ln q_e = \ln k_F + \frac{1}{n}\ln C_e \quad (4)$$

K_F and n are Freundlich constants, in which $1/n$, the heterogeneity factor, characterizes heterogeneous surface energy and K_F (mg/g (L/mg)$^{1/n}$) represents the adsorption capacity of the adsorbent.

Temkin and Pyzhev [27] considered that the heat of adsorption of all the molecules in the layer would decrease linearly with coverage due to some indirect adsorbent–adsorbate interactions. The Tempkin isotherm has been applied in the following form:

$$q_e = \left(\frac{RT}{b}\right)\ln K_T + \frac{RT}{b}\ln C_e \quad (5)$$

where b (J/mol) is the Tempkin constants, T (K) is the absolute temperature and R is the universal gas constant (8.314 J/mol). The plot of q_e vs. $\ln C_e$ can be used to find the isotherm constants.

The Langmuir, Freundlich, and Temkin isotherms constants are given in Table 3. As shown in Table 3, overall, the high regression coefficients ($R^2 > 0.99$) suggested that both Langmuir and Temkin models were suitable for describing the adsorption behavior of Cd (II) onto LSAC. However, the regression coefficients shown in Table 3 indicated that the Langmuir equation fitted the Cd(II) experimental data better at all temperatures (30, 40, 50°C), predicting the surface homogeneity of adsorbent and monolayer coverage of Cd(II) onto adsorbent. Similar results were also reported for Cd(II) adsorption elsewhere [19,28]. The adsorption capacity of LSAC increased slightly from 41.79 to 43.05 mg/g as the temperature increased from 25 to 55°C, showing that temperature was not a vital factor for Cd(II) adsorption onto LSAC. The value of 1/n gives an indication of the favorability of the adsorbent–adsorbate system. Values of $1/n < 1.0$ represent a favorable adsorption progress. Thus, the values of 0.4472–0.5085 showed favorable adsorption of Cd (II) onto LSAC.

Table 3
Isotherm model constants of three isotherm models for Cd (II) adsorption onto LSAC

Isotherms	parameters	Temperature (°C)		
		25	40	55
Langmuir	Q_0 (mg/g)	41.79	42.92	43.05
	K_l (L/mg)	0.0755	0.087	0.1137
	R^2	0.9989	0.9995	0.9992
Freundich	K_F (mg/g(L/mg)$^{1/n}$)	4.8502	5.6997	6.9392
	$1/n$	0.5085	0.4850	0.4472
	R^2	0.9665	0.9715	0.9712
Tempkin	K_T (L/mg)	0.7598	0.9278	1.2740
	b	273.72	273.67	285.19
	R^2	0.9962	0.9980	0.9978

3.6. Breakthrough studies

3.6.1. Effect of flow rate

The effect of flow rate was studied at 5, 10, and 15 mL/min while the inlet Cd(II) concentration was kept constant at 50 mg/L. The breakthrough curves at various flow rates are shown in Fig. 7. As can be seen, typical S-shaped breakthrough curves were presented. Initially the adsorption was very effective; almost no Cd(II) ions can be detected in the effluent. In the next stage of the process due to the gradual occupancy of active sites, the breakthrough point emerged. The effluent concentration of Cd(II) increased sharply after the breakthrough point. Then, saturation point was reached and the effluent approach to the feed concentration. Chu [29] considered that this type of breakthrough curve denoted the existence of either mass transfer limitation or flow nonidealities. The breakthrough curves shifted towards the origin with

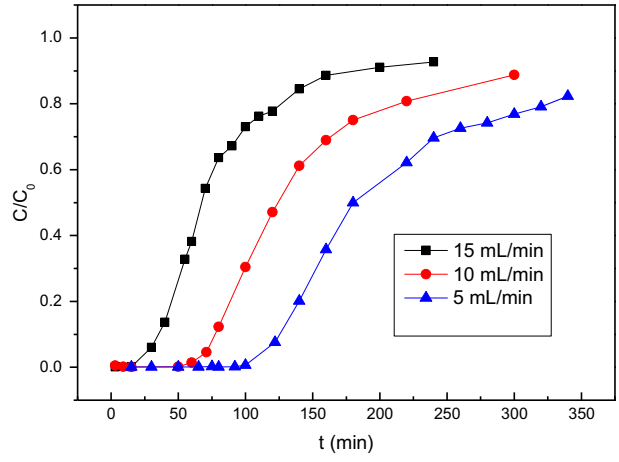

Fig. 7. Breakthrough curves for different flow rates (initial concentration = 50 mg/L; bed height = 6.5 cm; flow rate = 5, 10, 15 ml/min, $T = 25 \pm 1$ °C).

increasing flow rate. When the flow rate increased from 5 to 15 mL/min, the time required for complete column saturation decreased from 300 to about 150 min. An increase in flow rate increased the sharpness of the breakthrough curves. The curves displayed a sharp leading edge and a very broad trailing edge. This phenomenon can be explained by the slow intraparticle diffusion, which was a rate-limiting step and a slower approach of C/C_0 to unity also confirmed this point [30].

Effect of bed depth

Fixed-bed adsorption experiments were performed at bed heights of 3.9, 6.5, and 9.75 cm to investigate the effect of bed height (amount of LSAC loaded) on Cd(II) adsorption onto LSAC. The flow rate in fixed-bed experiments was kept at 10 cm^3/min and the initial concentration was 50 mg/L. The experimental breakthrough curves were shown in Fig. 8. As expected, the fixed-bed column with greater depth gave a later breakthrough. As the fixed-bed height increases, the contact time between Cd(II) in solution and sorbent increases, thus increasing the amount of Cd(II) solute retained in the LSAC adsorbent [31].

The Adams–Bohart model

Adams and Bohart discovered a model in 1920 to describe the relationship between C/C_0 and t in a gas–charcoal adsorption system. This model assumes that the adsorption rate is proportional to not only the residual capacity of the activated carbon but also the concentration of the adsorbing species. The Adams–Bohart model is used for describing the initial part of the breakthrough curve. In this work, the ability of Adams–Bohart model was evaluated for the relative concentration ranging from 0.01 up to 0.5 to describe the breakthrough behavior of LSAC. The equation had the following form [32,33]:

$$\ln\frac{C}{C_0} = k_{AB}C_0t - k_{AB}N_0\frac{Z}{U_0} \tag{6}$$

where N_0 is the adsorptive capacity (mg/L); C_0 is the influent concentration (mg/L); C is the effluent concentration (mg/L); t is the effluent time (min); Z is the bed depth of column (cm); U_0 is the linear velocity (cm/min); and k_{AB} is the kinetic constant of Adams–Bohart model (L/mg min), which represents the rate of solute transfer from the liquid phase to the solid phase. k_{AB} can be obtained from the slope of the plot of $\ln C/C_0$ vs. t and N_0 can be determined from the intercept of the plot. The average percentage errors (%) calculated by Eq. (7) below indicate the fit between the experimental and predicted values of C/C_0 used for plotting breakthrough curves. The parameters are listed in Table 4.

$$\varepsilon\% = \frac{\sum_{i=1}^{N}\left|\frac{(C/C_0)_{exp}-(C/C_0)_{cal}}{(C/C_0)_{exp}}\right|}{N}\times 100 \tag{7}$$

The subscripts "exp" and "cal" show the experimental and calculated values and N is the number of measurements.

The breakthrough data were fitted to the linear Adams–Bohart model. From Table 4, there is good agreement between the experimental and predicted values, suggesting that the Adams–Bohart model is valid for the relative concentration ranging from 0.01 up to 0.5 in this study. When the concentration was beyond this range, large discrepancies were found between the experimental and predicted curves for the Cd(II) adsorption in the fixed-bed column. As Table 4 displays, the adsorptive capacity increased and the adsorption rate constant decreased with the increasing flow rate, which was not in agreement with the results in literature [33]. The reason is that there may be differences in the adsorption mechanisms which cause the disagreement. While, the adsorptive capacity decreased with the increasing bed depth. So, a greater flow rate and a shorter bed depth of the parameter treated in this study would increase the adsorption of Cd(II) on the LSAC column.

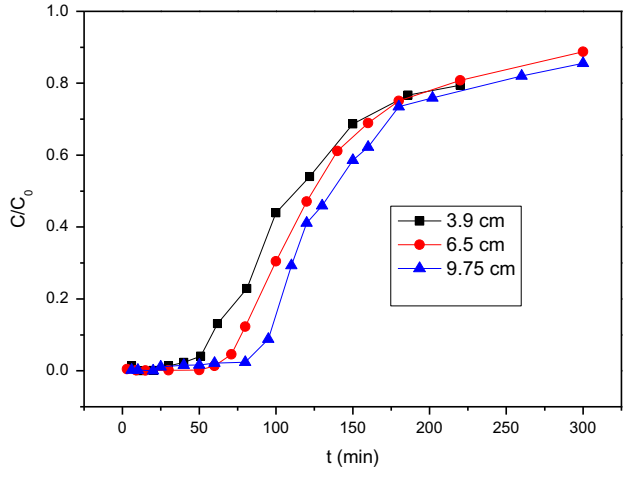

Fig. 8. Breakthrough curves for different bed heights (initial concentration = 50 mg/L; flow rate = 10 cm^3/min, bed height = 3.9, 6.5, 9.75 cm; $T = 25 \pm 1$°C).

Table 4
Parameters predicted from the Adams–Bohart model at different flow rates and bed depths

Bed depth (cm)	C_0 (mg/L)	Q (mL/min)	Adams–Bohart model		R^2	ε%
			k_{AB} (L/mg.min)	N_0 (mg/L)		
3.9	50	10	0.001028	284.0	0.9809	18.5
6.5	50	5	0.001232	56.8	0.9926	8.8
6.5	50	10	0.001136	193.4	0.9500	37.6
6.5	50	15	0.001013	451.8	0.9842	17.7
9.75	50	10	0.000775	128.9	0.9433	41.8

The relative concentration region is from 0.01 up to 0.5.

4. Conclusions

The activated carbon made from lotus stalks has a large BET surface area and pore volume. In the batch study, the metal uptake was found to increase with both temperature and pH, and the pH of the solutions influenced significantly the amounts of Cd (II) adsorbed by the LSAC. The pseudo-second-order kinetic model was found to provide better correlation with the adsorption kinetics data than the first-order one. The Langmuir model fits test data better than the Freundlich model or the Tempkin model. The Langmuir model predicted the Cd(II) adsorption capacity of the LSAC to be 41.79 mg/g at 25°C. In the continuous flow fixed-bed system, breakthrough curves were acquired for different liquid flow rates and bed heights. The Adams–Bohart model was found to be applicable and valid for the relative concentration ranging from 0.01 to 0.5 in this study. A greater flow rate and a lower bed depth would enhance the adsorption of Cd(II) on the LSAC column. In conclusion, this research evaluated the adsorption of Cd(II) by LSAC in batch and column experiments and showed that LSAC can be used as an effective adsorbent for the removal of Cd(II) from waste water.

Acknowledgment

The authors would like to acknowledge the financial support for this work provided by Shandong Province Postdoctoral Fund.

References

[1] K. Kadirvelu, C. Namasivayam, Activated carbon from coconut coirpith as metal adsorbent: Adsorption of Cd(II) from aqueous solution, Adv. Environ. Res. 7 (2003) 471–478.
[2] D. Feng, C. Aldrich, H. Tan, Treatment of acid mine water by use of heavy metal precipitation and ion exchange, Miner. Eng. 13 (2000) 623–642.
[3] Y. Fernández, E. Marañón, L. Castrillón, I. Vázquez, Removal of Cd and Zn from inorganic industrial waste leachate by ion exchange, J. Hazard. Mater. 126 (2005) 169–175.
[4] C.A. Kozlowski, J. Kozlowska, PNP-16-crown-6 derivatives as ion carriers for Zn(II), Cd(II) and Pb(II) transport across polymer inclusion membranes, J. Membr. Sci. 326 (2009) 215–221.
[5] S.W. Lin, R.M.F. Navarro, An innovative method for removing Hg^{2+} and Pb^{2+} in ppm concentrations from aqueous media, Chemosphere 39 (1999) 1809–1817.
[6] B. El-Eswed, F. Khalili, Adsorption of Cu(II) and Ni(II) on solid humic acid from the Azraq area, Jordan, J. Colloid Interf. Sci. 299 (2006) 497–503.
[7] I. Kula, M. Uğurlu, H. Karaoğlu, A. Çelik, Adsorption of Cd (II) ions from aqueous solutions using activated carbon prepared from olive stone by $ZnCl_2$ activation, Bioresour. Technol. 99 (2008) 492–501.
[8] T. Budinova, N. Petrov, J. Parra, V. Baloutzov, Use of an activated carbon from antibiotic waste for the removal of Hg(II) from aqueous solution, J. Environ. Manage. 88 (2008) 165–172.
[9] D. Borah, S. Satokawa, S. Kato, T. Kojima, Surface-modified carbon black for As(V) removal, J. Colloid Interf. Sci. 319 (2008) 53–62.
[10] W. Tongpoothorn, M. Sriuttha, P. Homchan, S. Chanthai, C. Ruangviriyachai, Preparation of activated carbon derived from *Jatrophacurcas* fruit shell by simple thermo-chemical activation and characterization of their physico-chemical properties, Chem. Eng. Res. Des. 89 (2011) 335–340.
[11] E.L.K. Mui, D.C.K. Ko, G. McKay, Production of active carbons from waste tyres—a review, Carbon 42 (2004) 2789–2805.
[12] N. Bagheri, J. Abedi, Preparation of high surface area activated carbon from corn by chemical activation using potassium hydroxide, Chem. Eng. Res. Des. 87 (2009) 1059–1064.
[13] T.G. Muhammad, Y. Chuah, A.R. Robiah, T.S.Y. Suraya, Choong Single and binary adsorptions isotherms of Cd(II) and Zn(II) on palm kernel shell based activated carbon, Desalin. Water Treat. 29 (2011) 140–148.
[14] L. Wang, J. Zhang, R. Zhao, Y. Li, C. Li, C. Zhang, Adsorption of Pb(II) on activated carbon prepared from *Polygonum orientale* Linn.: Kinetics, isotherms, pH, and ionic strength studies, Bioresour. Technol. 101 (2010) 5808–5814.
[15] L. Huang, Y. Sun, T. Yang, L. Li, Adsorption behavior of Ni (II) on lotus stalks derived active carbon by phosphoric acid activation, Desalination 268 (2011) 12–19.
[16] S. Chen, J. Zhang, C. Zhang, Q. Yue, Y. Li, C. Li, Equilibrium and kinetic studies of methyl orange and methyl violet adsorption on activated carbon derived from *Phragmites australis*, Desalination 252 (2010) 149–156.
[17] T. E. Kose, H. Demiral, N. Ozturk, Adsorption of boron from aqueous solutions using activated carbon prepared from olive bagasse, Desalin. Water Treat. 29 (2011) 110–118.
[18] S. Rengaraj, C.K. Joo, Y. Kim, J. Yi, Kinetics of removal of chromium from water and electronic process wastewater by ion exchange resins: 1200H, 1500H and IRN97H, J. Hazard. Mater. 102 (2003) 257–275.
[19] D. Mohan, K.P. Singh, Single- and multi-component adsorption of cadmium and zinc using activated carbon derived from bagasse—an agricultural waste, Water Res. 36 (2002) 2304–2318.

[20] G. Blázquez, F. Hernáinz, M. Calero, L.F. Ruiz-Núñez, Removal of cadmium ions with olive stones: the effect of somes parameters, Process Biochem. 40 (2005) 2649–2654.
[21] X.S. Wang, L.F. Chen, F.Y. Li, K.L. Chen, W.Y. Wan, Y.J. Tang, Removal of Cr (VI) with wheat-residue derived black carbon: Reaction mechanism and adsorption performance, J. Hazard. Mater. 175 (2010) 816–822.
[22] S. Lagergren, Zur theorie der sogenannten adsorption gelöster stoffe, K. Sven. Vetenskapsakad. Handl. 24 (1898) 1–39.
[23] Y. S. Ho, G. McKay, Pseudo-second order model for sorption processes, Process Biochechnol. 34 (1999) 451–465.
[24] M. Matheswaran, Kinetic studies and equilibrium isotherm analyses for the adsorption of methyl orange by coal fly ash from aqueous solution, Desalin. Water Treat. 29 (2011) 241–251.
[25] I. Langmuir, The adsorption of gases on plane surfaces of glass mica and platinum, J. Am. Chem. Soc. 40 (1918) 1361–1403.
[26] H. Freundlich, Adsorption in solution, Phys. Chem. Soc. 40 (1906) 1361–1368.
[27] M.I. Temkin, V. Pyzhev, Kinetic of ammonia synthesis on promoted iron catalysts, Acta Physiochim. 12 (1940) 327–356.
[28] Q. Tang, X. Tang, M. Hu, Z. Li, Y. Chen, P. Lou, Removal of Cd(II) from aqueous solution with activated Firmiana Simplex Leaf: Behaviors and affecting factors, J. Hazard. Mater. 179 (2010) 95–103.
[29] K.H. Chu, Improved fixed bed models for metal biosorption, Chem. Eng. J. 97 (2004) 233–239.
[30] D.O. Cooney, the importance of axial dispersion in liquid-phase fixed-bed adsorption operations, Chem. Eng. Commun. 110 (1991) 217–231.
[31] S.H. Kim, H.K. Shon, H.H. Ngo, Adsorption characteristics of antibiotics trimethoprim on powdered and granular activated carbon, J. Ind. Eng. Chem. 16 (2010) 344–349.
[32] Z. Aksu, F. Gönen, Biosorption of phenol by immobilized activated sludge in a continuous packed bed: Prediction of breakthrough curves, Process Biochem. 39 (2004) 599–613.
[33] R. Han, Y. Wang, X. Zhao, Y. Wang, F. Xie, J. Cheng, M. Tang, Adsorption of methylene blue by phoenix tree leaf powder in a fixed-bed column: Experiments and prediction of breakthrough curves, Desalination 245 (2009) 284–297.